PHYSICAL MODELING OF SAND LIQUEFACTION UNDER WAVE BREAKING ON A VERTICAL WALL

H. Michallet[1], V. Rameliarison[2] C. Berni[1], M. Bergonzoli[1], J.-M. Barnoud[1] and E. Barthélemy[1]

The wave induced liquefaction at a coastal structure is studied. Experiments in a glass-wall flume filled with a partially saturated bed of light-weight sediment are presented. Single wave loadings are simulated. For large enough wave height conditions an excess pore pressure is recorded within the soil and a liquefaction threshold is reached. Velocity fields obtained from video recordings display large zones of the bed that behave as a fluid. Phases of soil compaction and dilatancy are identified.

Keywords: Soil fluidization, pore pressure, momentary liquefaction, gas content.

INTRODUCTION

Wave forcing combined to coastline retreat may weaken or unsettle coastal and port structures. The combination of energetic flows and loose seabed mechanical properties at the vicinity of a structure may trigger scour and liquefaction phenomena leading to easier erosion (Sumer et al. 2001; de Groot et al. 2006). Former field experiments in a macro-tidal environment have shown that air bubbles can be trapped within the sand bed, as the beach de-saturates at low tide and partially saturates during rising tide (Breul et al. 2008). In these field experiments (Mory et al. 2007), liquefaction has been observed at the toe of a vertical wall subjected to intense wave forcing. The phenomenon was identified as momentary liquefaction (Sakai et al. 1992) and promoted by air bubbles trapped inside the bed. The seabed gas content is of major influence on pore pressure transmission and hence on liquefaction occurrence (Michallet et al. 2009). The criterion of liquefaction occurrence is estimated as the critical overpressure required to overcome the effective weight of the soil:

$$\Delta P = P_{i+1} - P_i > g\,\Delta z\,[\rho_s\,(1-n) + \rho_w\,n] \tag{1}$$

where P_i and P_{i+1} are the pore pressures at two depths in the sand bed, P_{i+1} being Δz below P_i, ρ_s and ρ_w are the densities of sediment and water, g is the gravitational acceleration, and n is the porosity.

Detailed measurements and visualization of the seabed are not easily obtained in the field. The present study aims at modelling the main physics of the seabed response to wave impact on a coastal structure. To that aim, a physical model using light-weight sediment is devised.

EXPERIMENTAL SET-UP

Experiments are carried out in a 11 m long flume, with glass-wall sides, one extremity consisting of a piston-type wave-maker and the other extremity closed by a Perspex vertical wall (see Figure 1). The bottom is covered with low-density ($\rho_s/\rho_w = 1.18$) sediment in a 1:20 sloping beach starting at 2 m from the wave-maker (see figure 1). Such light-weight sediment (median diameter 0.64 mm) has been used by Grasso et al. (2009) in order to scale wave-induced sediment transport processes. Different techniques for preparing a more compact or loose bed are tested, namely with dry or wet sand in an emptied flume or under water. Somehow the rising tide is simulated by filling the flume slowly with water after preparation of the beach. This allows air bubble trapping within the bed (gas content $C_g \sim 5\,\%$). Once the bed prepared and the water depth at the desired amount ($h_0 = 55.3$ cm at the wave-maker, 17 cm at the Perspex wall), the initial bed porosity is estimated to range from 0.43 (compact) to 0.52 (loose). The hydraulic conductivity of the bed has been estimated as $k = 3 \times 10^{-3}\,\mathrm{m\,s^{-1}}$. Pore pressures are measured at different depths in the soil against the wall (4 cm between sensors), capacitance gauges are used to measure free surface displacements. Furthermore, the different runs are video-recorded, with a focus on the bed region against the wall (25 cm in the x-direction and 12 cm in the vertical z-direction). The video camera has a resolution of 720×576 pixels (one pixel thus corresponds to about 0.6 mm), and

[1] CNRS/UJF/G-INP, UMR LEGI, BP53, 38041 Grenoble, France
[2] CETMEF/DS/LGCE, Technople Brest Iroise, BP5, 29280 Plouzané, France

a sampling of 25 images per second. Displacements fields are computed between two successive images with a Particle Image Velocimetry (PIV) software (Davis) in finding the best correlation over boxes of 16×16 pixels. Only motions in the bed are analysed.

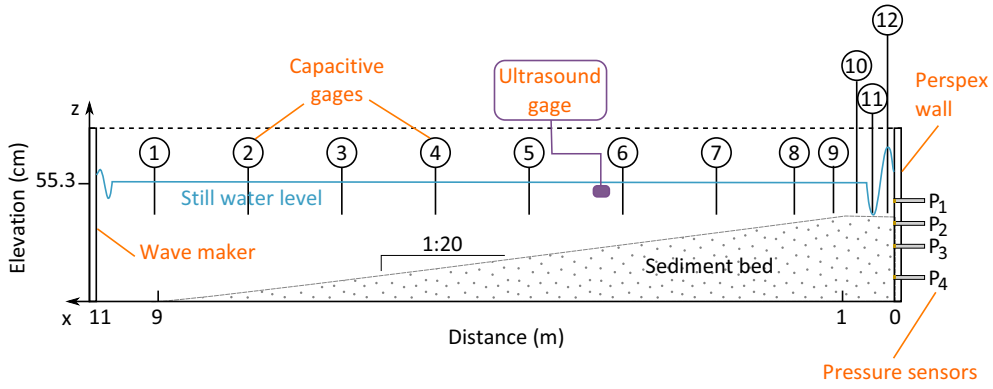

Figure 1. Schematic diagram of the experimental set-up: 12 capacitive gages measure free surface displacements, the ultrasonic gage mounted on a trolley enables bathymetric profiling, the pressure sensors measure the pore water pressure in between the sediment grains located against the vertical Perspex wall.

PORE PRESSURE MEASUREMENTS

With the aim of studying momentary liquefaction and therefore isolating the effect of wave impact, several wave-maker motions were tested. The chosen displacement of the piston consists of half a sine curve (2 s duration) starting with a backward motion. This generates a single wave consisting of a depression then an elevation of the free surface, followed by a small dispersive wave train. An example of the free surface elevations recorded along the flume is shown in Figure 2. When propagating on the sediment beach, the depression flattens and the elevation becomes steeper so that it breaks on the vertical wall at $t \simeq 6.5$ s. Note that there is a second wave of smaller amplitude impacting the wall at $t \simeq 9$ s. As seen from the signals for $t > 10$ s at the gauges the farthest from the wall, the main wave has lost most of its energy during the interaction with the wall.

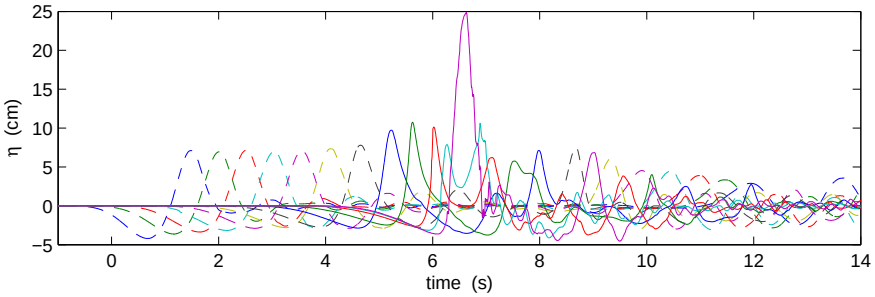

Figure 2. Surface elevations at $x = 9,\ 8,\ 7,\ 6,\ 5,\ 4,\ 3,\ 2,\ 1.35,\ 0.7,\ 0.35,\ 0.03$ m (measured by wave gauges $C1$ to $C12$, see Figure 1).

On top of Figure 3, the free surface elevation at the wall is plotted with the pore pressure measured at the bed, and within the soil. These measurements correspond to a very loose ($n \sim 0.52$) and unsaturated soil (gas content $C_g \sim 4\,\%$). After its first interaction with the wall, the wave train travels back and reflects on the wave-maker. Another interaction with the wall is recorded at $t \simeq 20$ s. Wave breaking is not observed during that interaction. At longer times, successive reflections with little dissipation occur on both flume extremities.

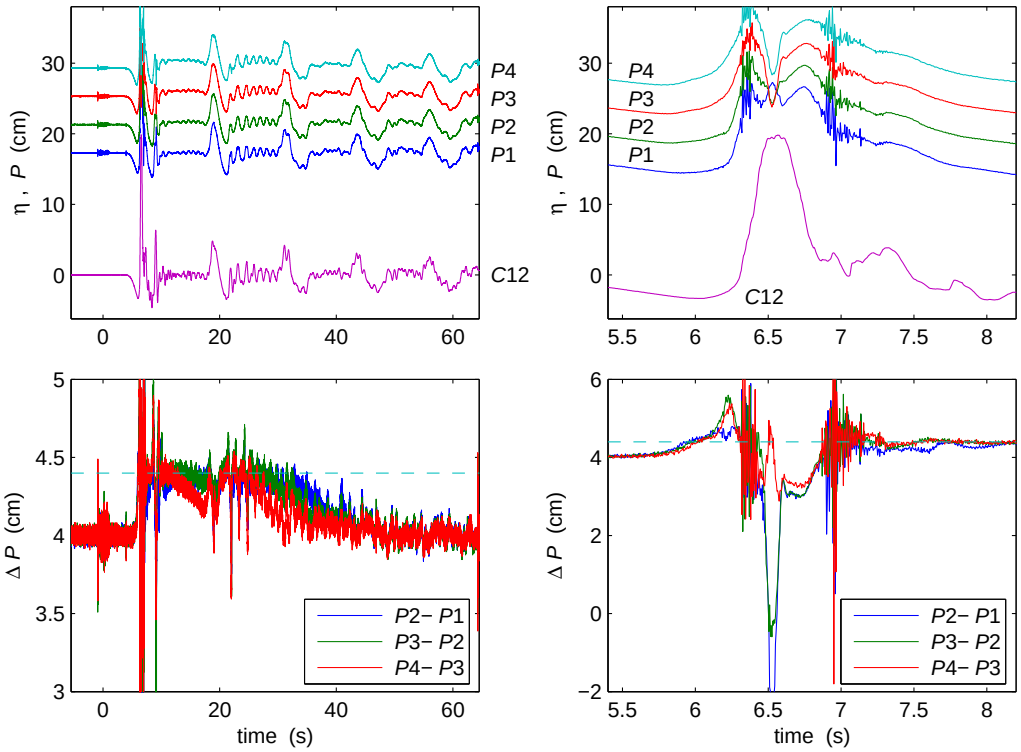

Figure 3. Pressure measurements against the wall, in a loose and unsaturated bed condition. Top: free surface elevation at the wall ($C12$), pore pressure at $z = 0,\ -4,\ -8,\ -12$ cm (from $P1$ to $P4$) below the sand bed (the water level at rest is at $z = 17$ cm). Bottom: pore pressure difference between two sensors. The horizontal dashed line corresponds to the threshold for liquefaction (1) for a porosity $n = 0.5$.

As seen on the top right pannel of Figure 3, during the rapid increase of the water level at first impact, high-frequency fluctuations in pore pressure are recorded. The general trend in pressure variation at the bed surface is similar to that observed for rigid bottoms (Peregrine 2003). In contrast, a pore pressure decay is recorded deep into the soil at approximately the same time as maximum water elevation. This pressure drop resembles to that recorded in the field experiments reported by Bonjean et al. (2004). High-frequency fluctuations are observed again as the water level decreases at the rear of the wave.

The bottom pannels in Figure 3 represent the pressure difference between two adjacent sensors. Prior to the wave, the pressure difference is equal to the hydrostatic pressure. With the wave of depression coming, the pressure difference for each layer of soil is increasing. It reaches the threshold of liquefaction that corresponds to the weight of the column of grains loosing contact, at $t \simeq 6$ s. Strong motions from the bed till 15 cm deep are visualized at this stage, as will be described in the next section. The pressure difference drops to negative values, likely due to changes in bed porosity. At $t \simeq 7$ s the liquefaction threshold is reached again. Then, as the bed is only slightly sheared by the low amplitude reflected waves, the grain settling takes place slowly and the hydrostatic pressure is recovered about 40 s later (bottom-left pannel in Figure 3).

The whole process leads to partial saturation of the soil. When the soil is liquefied, some air bubbles are escaping from the bed, as observed in the video recordings. The same run is repeated several times, each time after waiting long enough for the water surface to be perfectly still. Each wave interaction with the wall also results in a compaction of the soil. After 7 runs, the lowering of the bed at the wall is of about 3 cm. The decrease in porosity is approximately 20 % for the observed liquefied zone ($0 < x < 50$ cm, $0 > z > -12$ cm).

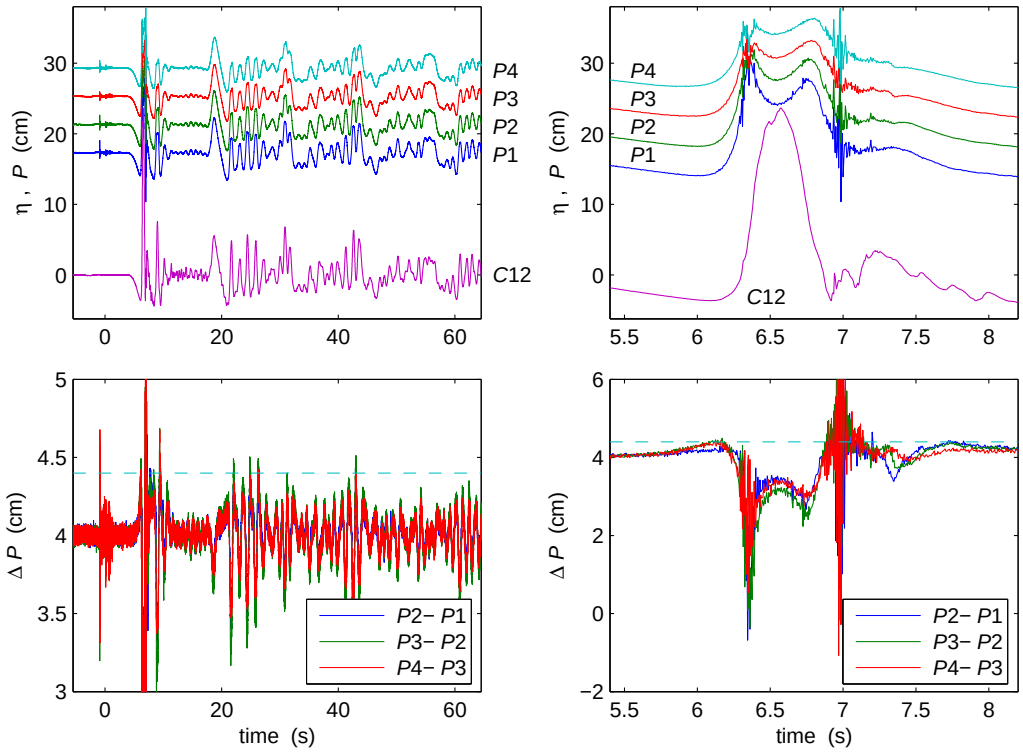

Figure 4. Pressure measurements against the wall, in more compact and saturated bed conditions in comparison with those of Figure 3. Top: free surface elevation at the wall ($C12$), pore pressure at $z = 0,\ -4,\ -8,\ -12$ cm (from $P1$ to $P4$) below the sand bed (the water level at rest is at $z = 17$ cm). Bottom: pore pressure difference between two sensors. The horizontal dashed line corresponds to the threshold for liquefaction (1) for a porosity $n = 0.5$.

The measurements of the last of the 7 runs are plotted in Figure 4. For this soil ($n \sim 0.43$, $C_g \sim 1\,\%$), the liquefaction threshold is hardly reached, and mainly at the rear face of the main wave (bottom right pannel). Overall, the pressure is more easily transmitted into the soil, that results in less wave damping compared to the case plotted in Figure 3. Here, grain motions are hardly detected in the soil. The bed level did not change as a result of that run.

OBSERVATION OF SOIL MOTION

Velocity fields of the sediment motion obtained during the first wave impact are shown in Figure 5. Against the wall, velocities are first oriented upwards as the bed liquefies ($t = 6.2$ s). Strong downwards velocities up to about $10\,\mathrm{cm\,s^{-1}}$ are then recorded at the wave crest ($t = 6.5$ s). After the wave crest, the flow reverses again. The 2D fields of

$$\tau = \sqrt{\frac{1}{2}\left[\frac{\partial u}{\partial x}^2 + \frac{\partial v}{\partial z}^2\right] + \frac{1}{4}\left(\frac{\partial u}{\partial z} + \frac{\partial v}{\partial x}\right)^2}\,, \tag{2}$$

which is proportional to the strain tensor modulus, the vorticity, and the divergence

$$\mathrm{div}\mathbf{U} = \frac{\partial u}{\partial x} + \frac{\partial v}{\partial z}\,, \tag{3}$$

computed from the horizontal (u) and vertical (v) velocities, are also shown. Large strain values are recorded at the wave impact. Cells of strong rotation are identified, indicating soil lenses moving as a

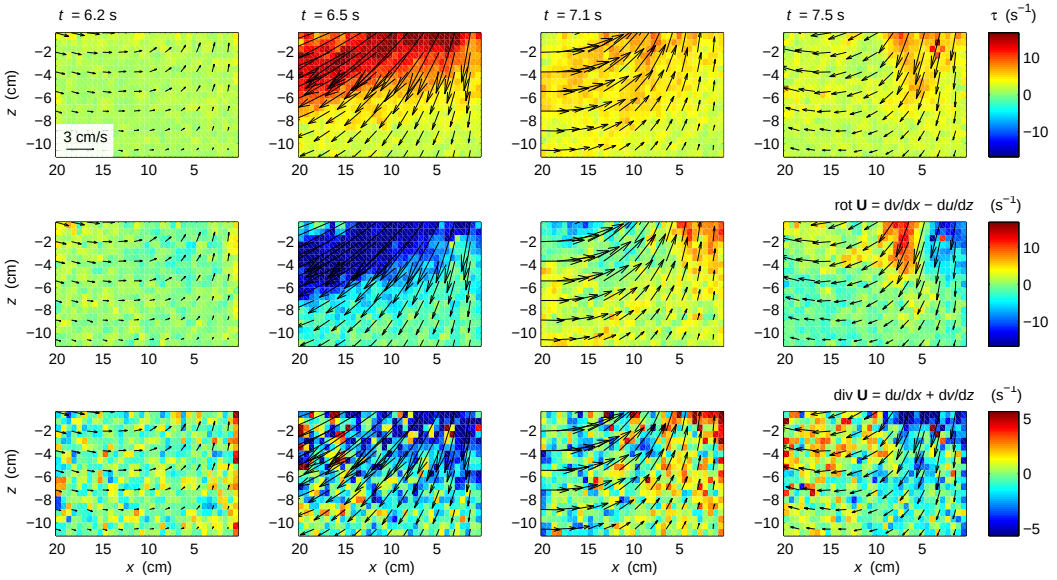

Figure 5. Particle Image Velocity fields of the sand grains motion at 4 stages of the wave impact on the wall, superimposed on the strain tensor modulus (top), vorticity (middle) and divergence (bottom). The wall is at $x = 0$, the bed level at $z = 0$.

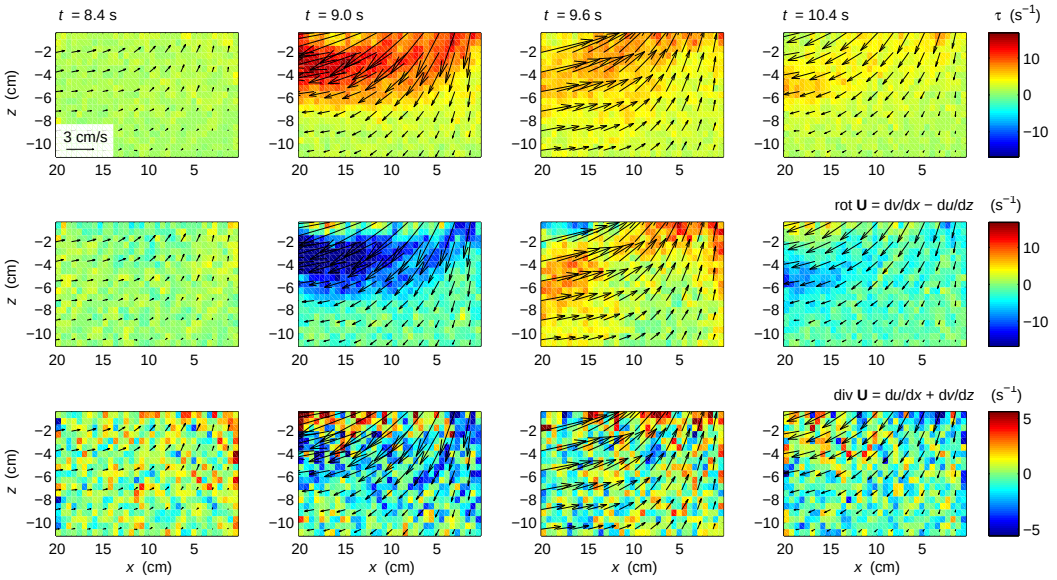

Figure 6. Same as in Figure 5, at 4 other stages.

block. The computation of the divergence indicates zones of dilatancy ($\mathrm{div}\mathbf{U} > 0$) against the wall as the soil first liquefies and just after the wave crest. Conversely, zones of compaction ($\mathrm{div}\mathbf{U} < 0$) are clearly identified at $t = 6.5\,\mathrm{s}$ and $t = 7.5\,\mathrm{s}$. A similar behaviour with reduced intensity is depitced in Figure 6, as the second smaller wave interacts with the wall.

The time series of pressure difference is plotted in Figure 7 along with the average values (over 11 cm deep and until 20 cm off the wall) of the strain tensor modulus, vorticity and divergence. For the divergence, the average over a zone closer to the wall is also computed. The times of large strain and vorticity clearly correspond to the wave impact and backwash. The second smaller wave has a similar signature (at $t \simeq 9$ and 9.5 s) to that of the main wave. The values of the divergence close to the wall clearly indicate the phases of dilatancy and compaction, in good agreement with the variations of the pressure measurements.

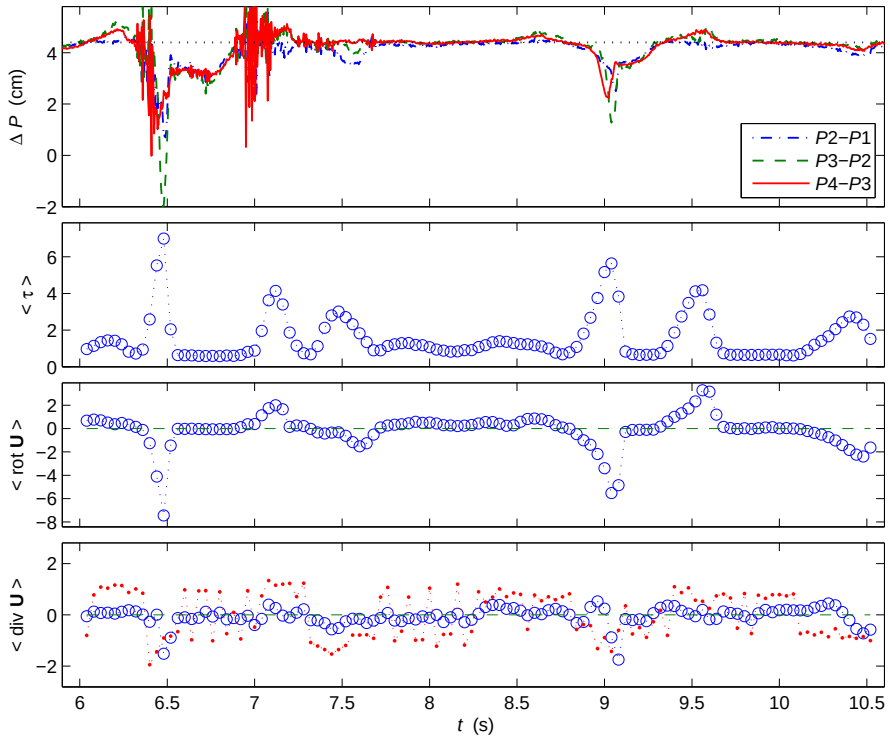

Figure 7. From top to bottom: time series of pressure difference at the wall; strain tensor modulus; vorticity; divergence. The quantities are averaged over the whole PIV field ($0 < x < 20$ cm, $0 > z > -11$ cm) shown in Figure 5 and 6 (circles) or restricting the area ($0 < x < 3$ cm, $0 > z > -11$ cm) close the wall (dots) for the divergence.

CONCLUSIONS

A physical model for studying liquefaction occurrence in the wave loading against a vertical wall was described. For large enough wave conditions, and for a loose and partially-saturated bed, an excess pore pressure is recorded within the soil and a liquefaction threshold is reached. A large zone of the bed then clearly behaves as a fluid. Sand grains displacements were quantified. Phases of soil compaction and dilatancy were identified. As runs are repeated, the bed becomes more compact and better saturated, and the liquefaction phenomenon no longer occurs.

Current research work aims at improving the quantification of the gas content and soil parameters in the experiments. Recently, Michallet et al. (2012) reported experiments in the same flume that reproduce liquefaction under cycling loading. The measurements are compared to the results of a coupled Discrete

Element Method - Pore-scale Finite Volume (DEM-PFV) model (Chareyre et al. 2012). The computation of the coupling between the flow and the motion of the particles enables to reproduce the excess pore pressure that lead to liquefaction, and the progressive compaction of the bed. By combining experimental and numerical approaches, a better knowledge of the wave conditions leading to liquefaction is foreseen.

ACKNOWLEDGMENTS

The technical support of L. Vignal, M. Lagauzère and F. Bonnel is gratefully acknowledged. J. Chauchat provided very useful comments on the computation of the strain modulus and estimation of the hindered settling. This work is funded by project Hydro-Fond (C2D2/RGCU, MEDDTL).

REFERENCES

Bonjean, D., P. Foray, I. Piedra-Cueva, H. Michallet, P. Breul, Y. Haddani, M. Mory, and S. Abadie. 2004. Monitoring of the foundations of a coastal structure submitted to breaking waves: Occurrence of momentary liquefaction, *Proc. 14th Int. Offshore Polar Eng. Conf.,* ISOPE, Volume 2, 585–592.

Breul, P., Y. Haddani, and R. Gourvès. 2008. On site characterization and air content evaluation of coastal soils by image analysis to estimate liquefaction risk, *Can. Geotech. J.,* 45(12), 1723–1732.

Chareyre, B., A. Cortis, E. Catalano, and E. Barthélemy. 2012. Pore-scale modeling of viscous flow and induced forces in dense sphere packings, *Transport in Porous Media,* 92, 473–493.

de Groot, M. B., M. B. Bolton, P. Foray, P. Meijers, A. C. Palmer, R. Sandven, A. Sawicki, and T. C. Teh. 2006. Physics of liquefaction phenomena around marine structures, *J. Waterw. Port Coastal Ocean Eng.,* 132(4), 227–243.

Grasso, F., H. Michallet, E. Barthélemy, and R. Certain. 2009. Physical modeling of intermediate cross-shore beach morphology: transients and equilibrium states., *J. Geophys. Res.,* 114, C09001, doi: 10.1029/2009JC005308.

Michallet, H., E. Catalano, C. Berni, B. Chareyre, V. Rameliarison, and E. Barthélemy. 2012. Physical and numerical modelling of sand liquefaction in waves interacting with a vertical wall, *Proc. 6th Int. Conf. on Scour and Erosion*, ICSE6–274.

Michallet, H., M. Mory, and I. Piedra-Cueva. 2009. Wave-induced pore pressure measurements near a coastal structure, *J. Geophys. Res.,* 114, C06019, doi: 10.1029/2008JC005071.

Mory, M., H. Michallet, D. Bonjean, I. Piedra-Cueva, J.-M. Barnoud, P. Foray, S. Abadie, and P. Breul. 2007. A field study of momentary liquefaction caused by waves around a coastal structure, *J. Waterw. Port Coastal Ocean Eng.,* 133(1), 28–38.

Peregrine, D. H.. 2003. Water-wave impact on walls, *An. Rev. Fluid Mech.,* 35, 23–43.

Sakai, T., K. Hatanaka, and H. Mase. 1992. Wave-induced effective stress in seabed and its momentary liquefaction, *J. Waterw. Port Coastal Ocean Eng.,* 118(2), 202–206.

Sumer, B. M., R. J. S. Whitehouse, and A. Torum. 2001. Scour around coastal structures: A summary of recent research, *Coastal Eng.,* 53, 965–982.